## **CONFERENCE PRE-PRINT**

# FAST ION TRANSPORT IN PRESENCE OF MAGNETIC PERTURBATIONS USING FULL-ORBIT AND GUIDING-CENTER SIMULATIONS

J.J. MARTINELL
Instituto de Ciencias Nucleares, UNAM
Mexico City, Mexico
Email: martinel@nucleares.unam.mx

L. CARBAJAL Type One Energy Oak Ridge, TN, USA

R. SAAVEDRA CICESE Ensenada, BC, Mexico

#### **Abstract**

Fast ion transport using two ways of describing particle motion is analyzed when there is a perturbation that produces magnetic islands. Particle trajectories are followed using the full orbit and with the guiding center approximation, comparing the respective results. Fast ions of energies typical of Neutral Beam Injection are released in a region internal to the island chain and the transport across the island is studied by measuring the ions in a radius external to the island. The results show that the guiding center (GC) simulations are less affected by the presence of the island than their full orbit (FO) counterparts. As expected, wider islands increase more the transport than narrow islands. Faster ions respond less to the island presence in FO but in GC it is the opposite. Allowing for island rotation, it is found that the flux across the island is reduced, with this effect being quite smaller in the GC than in the FO case. It is found that there is a resonant effect when the island rotation is of the order of the precession frequency of the trapped ions. When including the electric field associated with the island, there is an increase in radial transport due the three-dimensional nature of the field.

## 1. INTRODUCTION

In present fusion experiments the most common way of plasma heating is through neutral beam injection (NBI) or radio-frequency wave absorption (ICRF). This creates a population of high energy ions which has to be confined during the time they transfer the energy to the thermal plasma. When magnetic perturbations are developed in the plasma they modify the confining magnetic field and the transport of fast ions is modified. The perturbations due to tearing modes give rise to magnetic islands which increase the losses of fast ions. There can also be fast-ion losses due to instabilities or interactions with plasma waves that can lead to decreased confinement and energy losses. On the other hand, it has been predicted that fast ions can induce the formation of a transport barrier that improves plasma confinement [1].

Island rotation might also reduce the fast ion transport. This would be due to the effect of the radial electric field acting on the ion orbits. The question is whether the kind of flow intrinsic to magnetic islands has the ability to create a transport barrier for fast ions. That will depend on the type of magnetic islands present since they can be formed by neoclassical tearing modes (NTM) or created from the outside by resonant magnetic perturbations. However, for the case of rotating NTM an opposite effect has been found which increases, rather than reduces the ion losses, when the rotation frequency matches the precession frequency of trapped particles [2].

Here we focus on the transport of fast ions of the type used in NBI heating in medium-size tokamaks, that is, hydrogen ions with initial energies ranging from 10 keV to 50 keV. The influence of magnetic islands on the radial transport of the fast ions is explored by measuring the transport through the islands. A recent study [3] showed how magnetic perturbations of the type of RMP (Resonant Magnetic Perturbations) generated at the edge of the plasma might modify the transport of NBI ions. However, a detailed study about the relationship between the finite Larmor radius (FLR) of these ions and the effective size of the island produced by these MHD modes has not been performed. In the present work, we address this issue, showing that under certain circumstances fast ion confinement in presence of MHD modes can be degraded when the ion full orbit is followed, which includes FLR effects, in comparison with the guiding center description. We also find that, for rotating islands, an increased transport is observed at frequencies of the order of the ion precession frequency of trapped ions.

#### 2. SIMULATIONS DESCRIPTION

The two approaches are carried out with two codes that follow the fast ions: (1) using their full orbit with the KORC code [4, 5] and (2) with the guiding center equations in a toroidal magnetic field [6] with the GCAF code. For the simulations we use an analytical magnetic field corresponding to a tokamak with nested circular, toroidal magnetic flux surfaces, which in toroidal coordinates is given by:

$$\mathbf{B}(r,\theta) = [B_{\zeta}(r,\theta)\hat{\mathbf{e}}_{\zeta} + B_{\theta}(r,\theta)\hat{\mathbf{e}}_{\theta}]. \tag{1}$$

where  $B_{\zeta}(r,\theta) = B_0/(1+\epsilon\cos\theta)$  is the toroidal magnetic field,  $\epsilon = r/R_0$  is the inverse aspect ratio,  $R_0$  is the major radius at the magnetic axis,  $B_0$  is the toroidal magnetic field at  $R_0$ , and  $B_{\theta}(r) = \kappa\epsilon B_0/[q(r)(1+\epsilon\cos\theta)]$  is the poloidal magnetic field. Here  $\kappa = \hat{J}_p \cdot \hat{B}_{\zeta}$  with  $\hat{J}_p$  the unitary vector along the toroidal plasma current density. The safety factor is

$$q(r) = q_0 \left( 1 + \frac{r^2}{\varepsilon^2} \right) \,. \tag{2}$$

The constant  $\varepsilon$  is obtained from the values of  $q(r=0)=q_0$  and q(r=a) at the plasma edge r=a. The coordinates  $(r,\theta,\zeta)$  are defined as  $x=(R_0+r\cos\theta)\sin\zeta$ ,  $y=(R_0+r\cos\theta)\cos\zeta$ , and  $z=r\sin\theta$ , where (x,y,z) are the Cartesian coordinates with origin at the center of the torus. In these coordinates, r denotes the minor radius,  $\theta$  the poloidal angle, and  $\zeta$  the toroidal angle. Note that in this right-handed toroidal coordinate system, the toroidal angle  $\zeta$  rotates clockwise, that is, it is anti-parallel to the azimuthal angle,  $\phi=\pi/2-\zeta$ , of the standard cylindrical coordinate system.

The magnetic field of Eq. (1) is perturbed by including a single MHD mode [7] that can be written as follows:

$$\delta \mathbf{B} = \nabla \times \delta A \,, \tag{3}$$

where  $\delta A = \tilde{\alpha}(r,\theta,\zeta)R_0 \mathbf{B}(r,\theta)$ ,  $\tilde{\alpha}(r,\theta,\zeta) = \alpha(r)\cos\varphi_{mn}$ , with  $\varphi_{mn} = n\zeta - \kappa m\theta + \omega_{m,n}t$  and  $\alpha(r) = \alpha^*(r/r^*)[(a-r)/(a-r^*)]^p$  is the radial profile of the perturbation. Here, m and n are the toroidal and polodial wave numbers of the MHD mode,  $r^* = \varepsilon\sqrt{m/nq_0-1}$  is the radial position of the mode, where  $\alpha(r)$  reaches its maximum  $\alpha^*$ , and  $p = ma/r^* - m$ . This perturbation produces localized modes with magnetic islands of half-width

$$\delta r_{mn} \approx \sqrt{\frac{4q(r)b(r)R_0}{nq'(r)}}$$
, (4)

with q'(r) = dq(r)/dr, and  $b(r) = m\alpha(r)R_0/r$ .

Typical plasma parameters of a medium-size tokamak are used: toroidal magnetic field  $B_0=2$  T, major radius  $R_0=1.5$  m, plasma radius a=0.5 m,  $q_0=1$ ,  $q_a=5$ , which corresponds to a plasma current  $I_p\sim 300$  kA. The direction of the toroidal magnetic field  ${\pmb B}_\zeta$  is along the toroidal direction  $\hat{\pmb e}_\zeta$  and the plasma current density  ${\pmb J}_p$  is anti-parallel to  $\hat{\pmb e}_\zeta$ , therefore  $\kappa=-1$  in  $B_\theta(r,\theta)$  of Eq. (1). The bulk plasma is modeled as a hydrogen plasma, with electron thermal temperature of  $T_e=1$  keV and hydrogen ion temperature  $T_i=200$  eV. The number density of the plasma  $n_e$  takes the values  $10^{19}$  m $^{-3}$  and  $10^{20}$  m $^{-3}$  which has the effect of varying the collisionality of the fast ions with the bulk plasma.

The magnetic perturbation  $\delta \boldsymbol{B}$  has m=2 and n=1, while the amplitude  $\alpha^*$  takes the values  $\alpha^*=6.5\times 10^{-6}, 6.5\times 10^{-5}$  ( $\delta B/B_0\sim 10^{-4}$  and  $10^{-3}$ ). The corresponding island half-widths are  $\delta r=0.01, 0.03$  m, as predicted by Eq. (4).

In the simulations, for both full-orbit and guiding-center, we initialize the H ions with mono-energetic  $f(\mathcal{E})=\delta(\mathcal{E}-\mathcal{E}_0)$  and mono-pitch angle  $f(\eta)=\delta(\eta-\eta_0)$  distributions. The initial pitch angle is varied between,  $\eta_0=0^\circ,\ 30^\circ,\ 60^\circ;$  the zero pitch angle roughly resembles the case when the NBI ions are injected tangent to the local magnetic field while the others would represent oblique injection. Initially, ions are homogeneously distributed on a toroidal shell with minor radius r=0.19 m, centered at the magnetic axis  $R_0=1.5$  m, which is smaller than the island chain radius. Then, the ions are let to evolve for a slowing-down time  $\tau_s\sim 1/\nu_S$ , where  $\nu_S=\sum_s^{N_s}\nu_S^{is}$  is the slowing-down frequency due to collisions between the simulated ions species i and the bulk plasma species s. In all simulations we use  $10^4$  test particles for the fast ion population.

The bulk plasma conditions were set to a fixed temperature of  $T_e=T_i=1~\rm keV$  (like in an NBI plasma) and the density was varied in the range  $n_e=10^{19}-10^{21}~\rm m^{-3}$ . The fast-ion energy was taken to have the two values  $\mathcal{E}_0=10~\rm keV$  and 50 keV. On the other hand, the island parameters were taken as: (i) island width  $\delta=0.01,0.03$  m, (ii) island rotation frequency  $\omega=100~\rm rad/s$ ,  $1~\rm krad/s$ ,  $10~\rm krad/s$ .

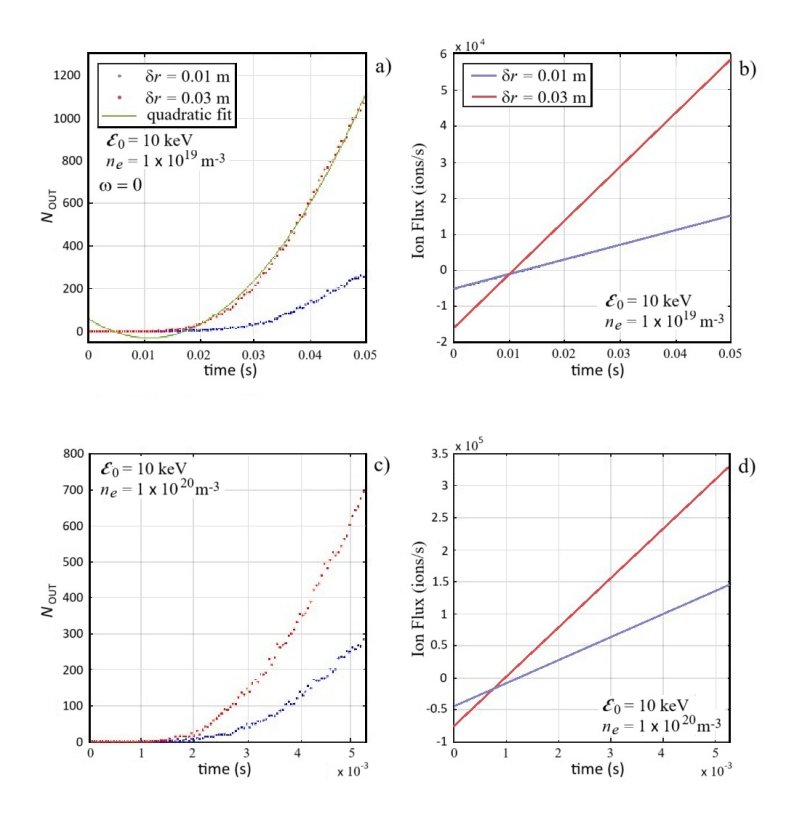


FIG. 1. Ion transport for FO across magnetic islands as function of the collisionality and magnetic perturbation intensity for ions with  $\mathcal{E}_0=10$  keV. Panel a): Number of particles crossing r=27 cm,  $N_{OUT}$ ,  $n_e=10^{19}$  m<sup>-3</sup> and 2 intensities of the magnetic perturbation. Total number of particles is  $10^4$ . Panel b): Ion flux through the flux surface q=2.2 computed using a quadratic fit of  $N_{OUT}$  in panel (a), shown with a green solid line. Panel c): same as panel (a) for  $n_e=10^{20}$  m<sup>-3</sup>. Panel d): same as panel (b) for  $n_e=10^{20}$  m<sup>-3</sup>.

### 3. TRANSPORT RESULTS

The ion flux across the magnetic island (at  $\rho^*=0.5$ , q=2), is measured by the time evolution of the number of ions crossing the flux surface at  $r\approx 0.27$  m:  $N_{OUT}(t)$ . The simulation is run up to the thermalization time of the fast ions, which for 50 keV ions is 150 ms for  $n=10^{19}m^{-3}$  and 15 ms for  $n=10^{20}m^{-3}$  while 10 keV ions thermalize in 50 ms or 5 ms for  $n=10^{19}m^{-3}$  and  $n=10^{20}m^{-3}$ , respectively. Because of the stochastic nature of the process the particles can cross radially in the positive or negative direction, so that  $N_{OUT}$  fluctuates around an average growing value. In Fig. 1 we show the FO time evolution of  $N_{OUT}$  for ions with  $\mathcal{E}_0=10$  keV and  $\mathcal{E}_0=50$  keV, respectively, with parallel injection, for two densities (different collisionality). Also, the size of the island is varied by modifying the amplitude of the perturbation  $\alpha^*$  of Eq. 3. Fig. 1(b) shows the flux of 10 keV ions for  $n=10^{19}m^{-3}$ , that is, ions per unit time  $dN_{OUT}/dt$  crossing the magnetic flux surface at q=2.2, computed by fitting a quadratic function to  $N_{OUT}$  in panel (a), and taking its first derivative. We observe that, for a fixed ion density, larger islands produce larger ion fluxes, as expected because the island shortcuts magnetic flux surfaces at two radii. Also, for a fixed island size, we observe an increase in ion flux when increasing the plasma density from  $n_e=10^{19}$  (panel (b)) to  $10^{20}$  (panel (d)). This is because the increased collisionality produces more radial transport.

For 50 keV ions a similar behavior is observed but with a reduced flux. This can be interpreted in terms of the collisionality since high-energy ions are less collisional and thus have reduced radial transport.

Next, the GC simulations are presented in Fig. 2. The fraction of particles crossing the island chain is shown as a function of time for the two energies 10 keV and 50 keV and two island widths, for the low density case, along with the normalized ion flux  $d(N_{OUT}/N)/dt$ . The ion flux is obtained from the parabolic fit curve to data. As with the FO simulations the ion flux increases as the perturbation strength is raised and the effect is larger for the lower energy. Also, for a given width, the absolute flux has a modest increase when the ion energy is increased. It can be appreciated that the fraction of particles crossing the magnetic island is quite larger in the FO simulations

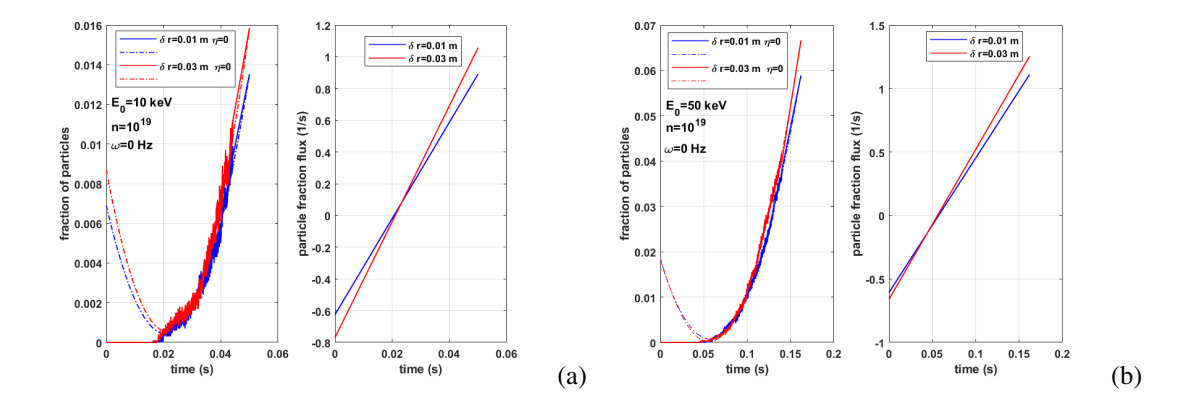


FIG. 2. Ion transport for GC across magnetic islands as function of the magnetic perturbation size for ions with  $\mathcal{E}_0=10$  keV (panel a) and 50 keV (panel b). Fraction of particles crossing the magnetic flux surface at r=27 cm and ion flux  $dN_{OUT}/dt$ , with  $n_e=10^{19}$  m<sup>-3</sup> and magnetic island widths 1 cm and 3 cm. Dotted lines are parabolic fits to data used to compute the ion fluxes.

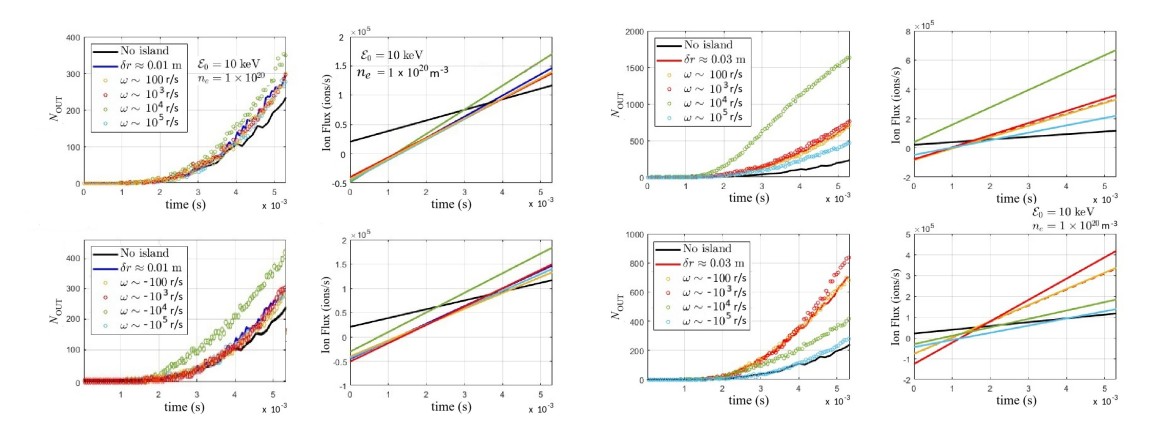


FIG. 3. Island rotation effect for rotation frequency between 100 rad/s and  $10^5$  rad/s for FO simulations. Narrow and wide islands are in left and right panels respectively, for co- (top) and counter- (bottom) rotation. Ion energy is 10 keV and  $n=10^{20}m^{-3}$ . Black line is for no perturbation while the color line is for a static island.

than in the GC cases. The dependence with density is also similar in the two types of simulations. The fact that the ion energy dependence does not have the same trend in GC as in FO simulations may be due to the fact that GC orbits follow field lines and hence radial transport is not so dependent on the collision rate; FLR is not included.

#### 3.1. Island rotation

We now include island rotation in the plasma frame of reference taking  $\omega \neq 0$  in Eq. 3. The rotation can be either in the direction of the ion rotation (co-rotation  $\omega > 0$ ) on in the opposite direction (counter-rotation  $\omega < 0$ ). An important difference between FO and GC results is that, for the GC there is almost no difference when the rotation velocity sign is changed, whereas for FO the fluxes show a significant difference as shown in Fig. 3. In this figure we show the time evolution of  $N_{OUT}$  and the ion flux for a plasma with density of  $10^{20}m^{-3}$  for ions of energy 10 keV, for the two island widths (left and right panels respectively); co-rotation is in the upper panels and counter-rotation in the lower panels, with different magnitudes of the rotation frequency. The results for a static island and without island are also shown. The difference in the flux due to rotation is more important for a wide island, in which case the transport through the island tends to be reduced (except for some cases to be discussed below) in a proportion that is larger for counter- than for co-rotation. It is also observed that, for some rotation frequencies, the fast ion flux can be close to the values obtained when there is no island. Interestingly, some of our results show that, for narrow islands with counter-rotation, the flow can be even lower than the one with no islands. These islands would then act as some kind of transport barrier.

Regarding the influence of the magnitude of the rotation frequency on the flux, the behavior is dependent on the

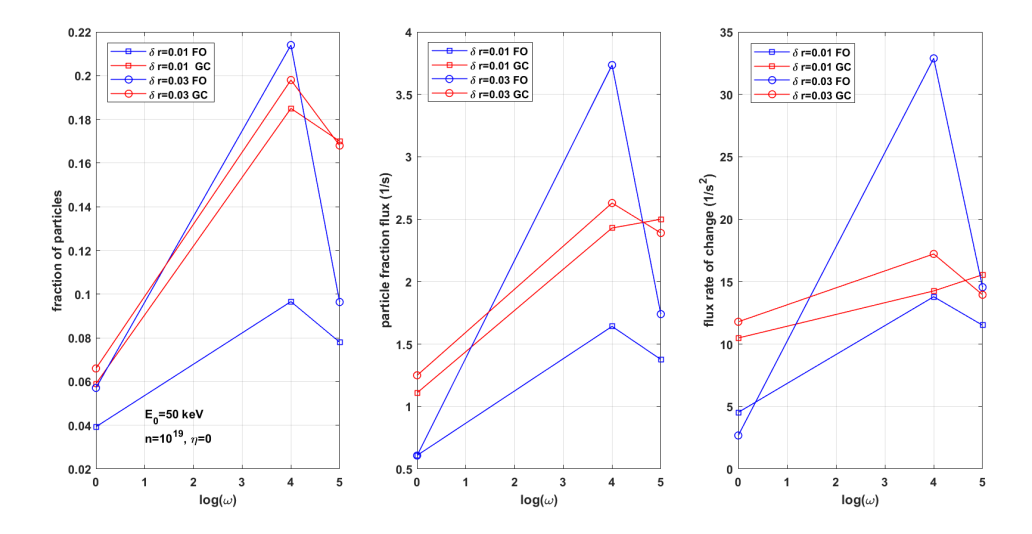


FIG. 4. Particle fraction at the final time, after thermalization, as function of the rotation frequency. Second panel shows the ion flux  $d\hat{N}/dt$  and the last panel is the flux rate of change:  $d^2\hat{N}/dt^2$ , for 50 keV ions in a plasma with  $n=10^{19}m^{-3}$ . The initial pitch angle of the ion beam with respect to the magnetic field is  $\eta=0$ ; and they are shown for two island widths. Results for GC (red) and FO (blue) are compared.

rotation sign. In the co-rotating island of the upper panels of Fig. 3 the flux increases with the rotation frequency up to a maximum value for  $\omega=10^4$  rad/s but it then decreases when the rotation increases more. This occurs for the narrow and the wide islands but is more pronounced for the large perturbation. The same effect is observed for the higher energy ions with 50 keV, see Fig. 4. This suggests that there is a resonant effect at  $\omega\approx10^4$  rad/s (it may be different for the higher energy ions but within the same order of magnitude). This frequency is smaller than the transit frequency for the passing ions with zero pitch angle which, for  $\mathcal{E}_0=10$  keV at r=a/2 is  $\omega_t=v/Rq=4.6\times10^5 s^{-1}$  and for  $\mathcal{E}_0=50$  keV is  $\omega_t=1\times10^6 s^{-1}$ . The trapped ions bounce frequency is  $\omega_b=\pi v\sqrt{2\epsilon}f(\eta)/4qR\leq1.2\times10^5 s^{-1}$ , for 10 keV ions at r=a/2. However they also have a precession frequency which can be close to  $10^4 s^{-1}$  and resonate with the island rotation frequency. The resonant flux increase of the trapped ions may be due to the an increase of the parallel velocity by the in-phase rotating island in each precession period, making the island crossing more efficient.

On the other hand, for counter-rotation (lower panels in Fig. 3) the flux is similarly affected by rotation for the narrow island. For the wide island, the flux is reduced from the static island vales for most rotation frequencies, except for  $\omega=-10^3$  rad/s, as opposed to co-rotation where most frequencies produce flux increase except when  $\omega=-10^5$  rad/s. Flux reduction would be expected if rotation made more difficult to follow the magnetic field lines of the island separatrix. Notice that the maximum flux for a wide island is for  $\omega=-10^3$  rad/s. instead of the resonant frequency of  $\omega=10^4$  rad/s found in co-rotation, which is still the same for the counter-rotating narrow island ( $\omega=-10^4$  rad/s). In these cases the flux is larger than the static island flux. Then, counter-rotation exhibits again the resonant increase of ion flux. As before, trapped particles would resonate with island rotation at their precession frequency. However, the frequency would not necessarily be the same, because of the interaction between trapped and circulating ions. That may explain why we found that the resonance is the same as in co-rotation for a narrow island but it has smaller frequency ( $\omega \sim 10^3$  rad/s) for wide islands.

For the GC simulations the resonance effect is still there but less conspicuous. The comparison between the FO and GC cases can be seen in Fig. 4 where the final ion fraction  $\hat{N}=N(t=t_f)/N_{OUT}$ , the final ion fraction flux  $\hat{\Gamma}=(d\hat{N}/dt)(t=t_f)$  and the flux rate  $d\hat{\Gamma}/dt$ , are plotted as functions of the rotation frequency. Here we show the results for the rotation frequencies  $\omega\approx 0$ ,  $10^4$ , and  $10^5$  rad/s. The dependence on perturbation amplitude and initial pitch angles is presented. The ion energy is 50 keV and the plasma density is  $n=10^{19}m^{-3}$ . The resonant effect for  $\omega\approx 10$  krad/s is observed in all cases although it is much less pronounced for the GC results.

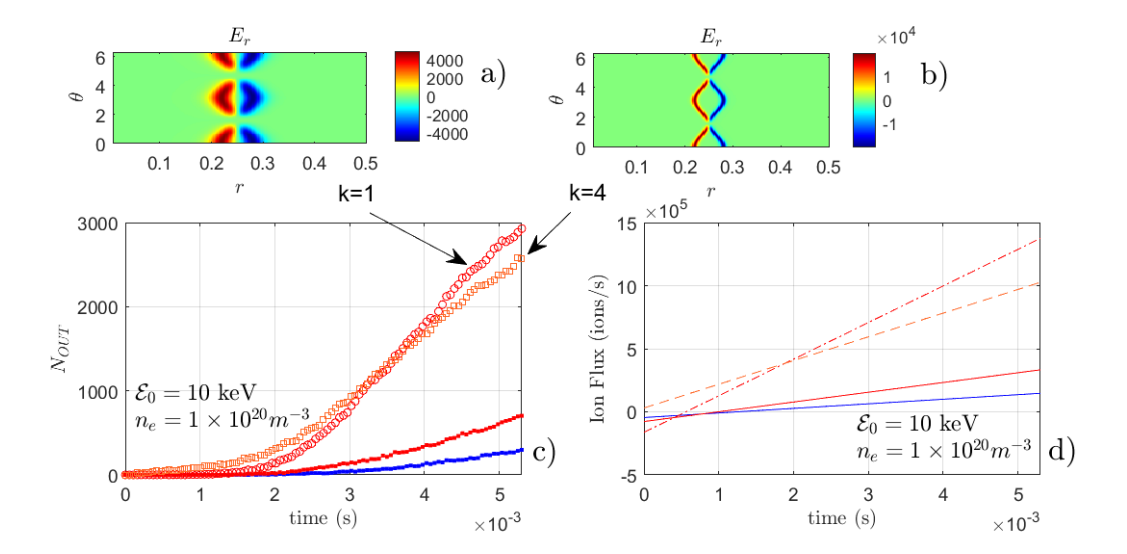


FIG. 5. Island electric field effect on the ion flow for k=1 and 4 using FO. Continuous red line is for an island of width  $\delta=0.03$  m without electric field. Blue line is with no island. Red symbols is for the wide potential shown in panel (a) while orange is for narrow potential in panel (b). (c) and (d) panels show number of particles crossing the island and the corresponding ion flux. The island has no rotation,  $\mathcal{E}_0=10$  keV,  $n_e=10^{20}$  m<sup>-3</sup>.

#### 3.2. Island electric field

Thee island has electric potentials associated with it due to the transport processes in the perturbed magnetic field. The electric potential can be modeled by

$$\phi(r,\theta,\zeta) = \phi_0 \left( 1 - \frac{1}{1 + \exp\left\{ -k\left( r - ro - d\left( 1 - \cos^2 \varphi_{mn} \right) \right) \right\}} - \frac{1}{1 + \exp\left\{ k\left( r - ro + d\left( 1 - \cos^2 \varphi_{mn} \right) \right) \right\}} \right)$$
(5)

where,  $\varphi_{mn} = \frac{m}{2}\kappa\theta - \frac{n}{2}\zeta + \omega_{m,n} - \omega t$ . It is characterized by the parameters k and d, measuring the breadth around the island separatrix affected by the electric field and the half-width of the field region, respectively. The latter is taken to be equal to the island width  $d = \delta r_{mn}$ .

The electric field in this model is not just radial but it has a 3D structure. This means that the  $\mathbf{E} \times \mathbf{B}$  drift for the ions is not poloidal but has some radial component. When the electric field is radial, the electric drift produces a poloidal plasma flow which tends to reduce the radial transport. But here, the 3D structure would produce radial flows across the island.

In FO simulations the electric field effect on the fast ion transport across the island when there is no rotation is shown in Fig. 5. It is clear that the flux is increased when the island electric potential is included, for two electric field breadths (k = 1, 3). The figure also presents the geometric structure of the electric field. The wider the electric field region the larger the long-term ion flux, although initially it is harder for particles to cross the region. Notice the increased flow through the island region as a result of the 3-dimensional structure of the electric field.

#### 4. DISCUSSION AND CONCLUSIONS

We now make a closer comparison of FO and GC results. First we focus on the effect of changing the initial pitch angle, which so far has been kept equal to zero. Increasing the pitch angle  $\eta$  has the effect of making the finite Larmor radius dynamics more important. Thus, the possible advantages of using FO over GC simulations are more apparent. For FO, the effect of  $\eta$  is to increase the flux since the FLR is larger but as FLR grows a steadier flux is reached. As mentioned before, FO simulations produce an increase in the radial flux as the fast ion energy is reduced or when density increases. On the other hand, again the GC fluxes are not very sensitive to the variations of either pitch angle or island width. This is an indication of the importance of the finite Larmor radius. An interesting result is that the GC flux is larger than the FO flux at the resonant frequency for small island width, while for large island width the GC flux is smaller. This is because in FO cases the flux decreases when there is rotation together with the almost unnoticed effect of rotation in the GC case.

Next, the effect of density is to increase the ion outflow but not the fraction of crossing ions, for both FO and GC

### MARTINELL ET AL.

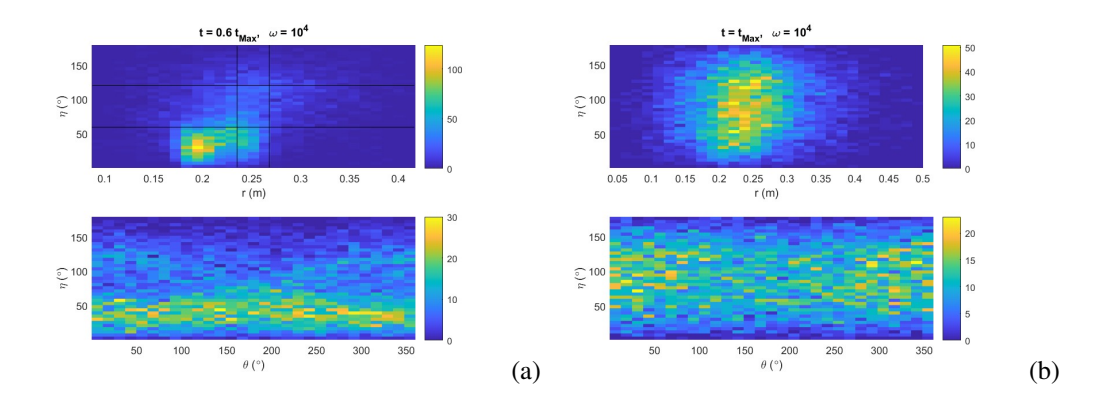


FIG. 6. Ion population as function of pitch angle and radius for two times (a)  $t = 0.6t_{Max}$  and (b)  $t = t_{Max}$  where  $t_{Max}$  is the final simulation time (thermalization). These are FO simulations of 10 keV ions with an island width  $\delta = 0.03$  m rotating at the resonant frequency 10 krad/s,  $n = 10^{19} m^{-3}$ . The highlighted region signals the region where trapped ions and coincide with the island position.

simulations. This is because at high density the ions thermalize in a short time and not many of them can cross the island, even though the transport is larger than for low density.

Regarding the sensitivity to the parameters characterizing the electric potential, the ion flux for the low ion energy ions is lower for the value k=4 (short breadth) than for smaller k. In contrast, for energy 50 keV there is almost no difference when k is changed.

The differences between FO and GC simulations may be related to the breakdown of perturbative guiding-center models [8], including the one used in this work, for accurately describing the dynamics of energetic particles. It is important to mention that, despite using higher order perturbative guiding-center models, important differences between FO and GC dynamics are still observed. In this reference it is shown that, for cases where the smallness parameter used to derive perturbative guiding-center models,  $\epsilon = r_L/L_0$ , where  $L_0 \sim 0.01$  m is the characteristic length scale of the magnetic field perturbation, exceeds  $\sim 10\%$ , these perturbative guiding-center models show important deviations from the FO dynamics dictated by the full Lorentz force. For the cases studied here of 10 keV and 50 keV ions,  $\epsilon \sim 50\%$  and 100%, respectively. Therefore, discrepancy between FO and GC estimates is expected. In Ref. [9] it is also shown that the adiabaticity is not preserved in GC theory for high frequency fluctuations above a threshold amplitude. In these cases, FO description which does not rely on adiabaticity should be used.

Lastly, we can attempt to find the possible reason for the resonant increase of ion flux at  $\omega \sim 10$  krad/s. Thus, we have analyzed the behavior of the fast ions interacting with the island based on our simulations. Similar results have also been found in previous works like Refs. [2] and [10]. Bardoczi et al [10] found that the phase space wave-particle resonances are dependent on the island rotation frequency and lead to an increase in the fast ion losses with frequency. The resonance is found when a core resonance is formed which leads to an improvement in fast ion confinement as the frequency rises. Ferrari et al.[2] found that the resonance is related to the toroidal precession frequency of the trapped ions. Accordingly, we look for a correlation between trapped ions and the rotating island. Thus, we have plotted the ion pitch angle (velocity variable) versus the radius (space variable) for different frequencies and different times during the simulation. Additionally, plots of toroidal angle versus poloidal angle give information about the ion spatial distribution.

For FO simulations, figure 6 shows the plots of  $\eta$  vs r and  $\eta$  vs  $\theta$  for two an intermediate time and for the final time (thermalization time) for 10 keV ions with a wide island,  $\delta=0.03$ m, rotating at the resonant frequency,  $10^4$  rad/s. It is seen that, during the evolution towards thermalization, there is evidence that a trapped ion population develops in coincidence to the island position at time 0.6 the thermalization time. This is because the region of ion trapping which is highlighted by the horizontal black lines, straddling  $\eta=90^\circ$ , has a significant ion population at the region of the island  $r=0.25\pm0.015$  m, marked with the vertical black lines. This only appears around this time since by the end of the simulation, the pitch angles cover the whole range, with no distinction for trapped ions. The effect is not strong because only a small fraction of the ion population has reached the island, while the bulk of the population stays close to their release surface. But there is a sizable population in the relevant region that provide evidence that trapped ions are interacting with the rotating island. When the rotation frequency is changed from the resonance value these effects are not observed.

The second result comes from the  $\theta$  vs  $\zeta$  plots shown in Figure 7. Here the same times for the same simulation

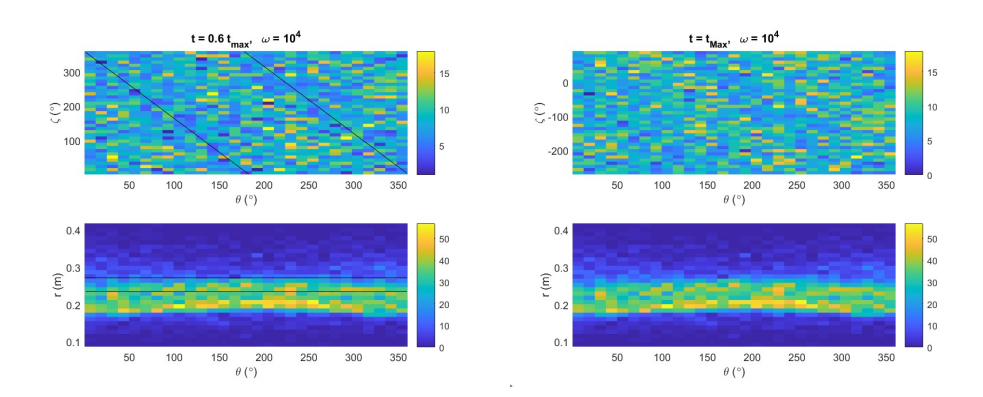


FIG. 7. Ion population for  $\theta$  vs  $\zeta$  and for  $\theta$  vs radius for 2 times,  $t=0.6t_{Max}$  and  $t=t_{Max}$  where  $t_{Max}$  is the final time. FO ions of 10 keV with island width  $\delta=0.03$  m at the resonant  $\omega=10$  krad/s,  $n=10^{19}m^{-3}$ . The helical path of the island is highlighted with the lines. Ion bunching along them is seen for  $t=0.6t_{Max}$ .

are presented and it is seen that there is evidence of ion bunching along the helical direction of the island. This is marked by the black lines. Although the effect is quite dim, the green areas seem to be aligned with the rational surface where the island is located. This is only observed for the intermediate times. before thermalization destroys it. Again, for the other frequencies this alignment does not occur.

The same resonant effect is observed for 50 keV ions, as expected, because the same behavior is seen for both energies. This analysis gives insightful evidence of the role of trapped ions in the resonant process. This helps to understand some of the underlying causes.

ACKNOWLEDGEMENTS. Support from UNAM-DGAPA PAPIIT project IN105125 is greatfully acknowledged.

### **REFERENCES**

- [1] A. Di Siena, R. Bilato, T. Görler, A. Bañón Navarro, E. Poli, V. Bobkov, D. Jarema, E. Fable, C. Angioni, Ye.O. Kazakov, R. Ochukov, P. Schneider, M. Weiland, and F. Jenko. New high-confinement regime with fast ions in the core of fusion plasmas. *Phys. Rev. Lett.*, 127:025002, 2021.
- [2] H.E. Ferrari, R. Farengo, P.M. Garcia, and C.F. Clauser. Trapped particle resonance effects on the ntm driven losses of energetic particles. *Plasma Phys. Control. Fusion*, 65:025001, 2023.
- [3] G.J. Kramer, R.V. Budny, A. Bortolon, E.D. Fredrickson, G.Y. Fu, W.W. Heidbrink, R. Nazikian, E. Valeo, and M.A. Van-Zeeland. A description of the full-particle-orbit-following spiral code for simulating fast-ion experiments in tokamaks. *Plasma Phys. Control. Fusion*, 55:025013, 2013.
- [4] L. Carbajal, D. Del-Castillo-Negrete, D. Spong, S. Seal, and L. Baylor. Space dependent, full orbit effects on runaway electron dynamics in tokamak plasmas. *Phys. Plasmas*, 24:042512, 2017.
- [5] D. Del-Castillo-Negrete, L. Carbajal, D. Spong, and V. Izzo. Numerical simulation of runaway electrons: 3-d effects on synchrotron radiation and impurity-based runaway current dissipation. *Phys. Plasmas*, 25:056104, 2018.
- [6] R.B. White. The theory of toroidally confined plasmas, 2nd ed. Imperial College Press, London, 2006.
- [7] H.E. Mynick. Transport of energetic ions by lown magnetic perturbations. *Phys. Fluids B*, 5(5):1471–1481, 1993.
- [8] J.W. Burby, I.A. Maldonado, M. Ruth, D.A. Messenger, and L. Carbajal. Non-perturbative guiding center model for magnetized plasmas. *Phys. Rev. Lett.*, Accepted, 2025.
- [9] H. Chen, L. Chen, F. Zonca, J. Li, and M. Xu. Validity of gyrokinetic theory in magnetized plasmas. *Commun. Phys.*, 7:261, 2024.
- [10] L. Bardoczi, M. Podesta, W.W. Heidbrink, and M.A Van Zeeland. Quantitative modeling of neoclassical tearing mode driven fast ion transport in integrated transp simulations. *Plasma Phys. Control. Fusion*, 61:055012, 2019.